



## Ore-forming mechanism of Xiajinbao gold deposit in Pingquan, Hebei based on fluid inclusions and stable isotopes

Jian-guo ZHANG<sup>1,2,3</sup>, Yong-jun SHAO<sup>1,2</sup>, Cheng WANG<sup>1,2</sup>, Zhong-fa LIU<sup>1,2</sup>, Yi-qu XIONG<sup>1,2</sup>

1. Key Laboratory of Metallogenic Prediction of Non-ferrous Metals and Geological Environment Monitoring, Ministry of Education, Central South University, Changsha 410083, China;
2. School of Geosciences and Infophysics, Central South University, Changsha 410083, China;
3. China Nonferrous Metals Resource Geological Survey, Beijing 100012, China

Received 13 August 2016; accepted 1 April 2017

**Abstract:** The Xiajinbao gold deposit is located in Yong'an—Xiayingfang—Maojiagou polymetallic metallogenic belt, which is an important metallogenic belt in North China block. In this paper, we present a detailed study on fluid inclusions and stable isotopes of the Xiajinbao gold deposit, Hebei Province, China, aiming at discussing the ore source, evolution of ore-forming fluid and ore-forming mechanism of the deposit. The macroscopic geological characteristics, S and Pb isotopic analysis results show that the source of ore-forming materials is mainly from granitic magma, and subordinately from country rocks. H and O isotopic composition features indicate that the ore-forming fluid is mainly derived from magmatic water. Fluid inclusion characteristics show that the ore-forming fluid experienced boiling during the early mineralization stage, which led to the precipitation of gold. Fluid mixing dominated the precipitation of the ore-forming materials during the middle and late stages. The gold precipitation was caused by water/rock reaction throughout the whole ore-forming process.

**Key words:** fluid inclusion; stable isotopes; ore-forming source; ore-forming mechanism; Xiajinbao gold deposit

### 1 Introduction

The Xiajinbao gold deposit (also known as Xiayingfang gold deposit), is located in the northeastern margin of the Longxutai Mesozoic sub-volcanic basin in the North China block, and belongs to the Xiayingfang gold ore district [1]. It is one of the most important part of the Yong'an—Xiayingfang—Maojiagou tectonic-magmatic activity zone, and hosted in the triple joint position among the North China plate, Siberia plate and Pacific plate [2,3]. During the Mesozoic, the area entered an intra-plate orogenic stage of intensive tectonic magmatic activities, which were associated with Au–Mo–Cu–Pb–Zn–Ag mineralization [4,5].

There are some previous studies on the Xiajinbao gold deposit and its adjacent areas. LUAN and YU [1] studied the types and homogenization temperatures of the fluid inclusions in the gold-bearing quartz veins of the Xiajinbao deposit, China, and concluded that the ore-forming temperatures fall into the middle and low

temperature ranges. YUAN et al [6] considered that the mineralization began in 153.9 Ma, based on the fission track age of the zircon and apatite. The LA-ICP-MS zircon U–Pb chronological analysis indicated that the age of Xiajinbao granitic porphyry is 158 Ma [7]. As can be seen from the above, the source of ore-forming materials, the source and evolution of ore-forming fluid, and the ore-forming mechanism are still unclear. Especially few studies have examined the controlling factors of the precipitation of gold in this area. Therefore, this paper combined with the fluid inclusion features and H, O, S, Pb isotopic compositions with detailed field investigations to systematically study the source of ore-forming materials, the source and evolution of the ore-forming fluid, and the ore-forming physiochemical conditions of the Xiajinbao gold deposit. The controlling factors of the gold precipitation and the ore-forming mechanism of Xiajinbao gold deposit were discussed. It will enrich the metallogenic theory of gold deposit in this area, and provide theoretical support for future exploration and prospecting work in deep and boundary area.



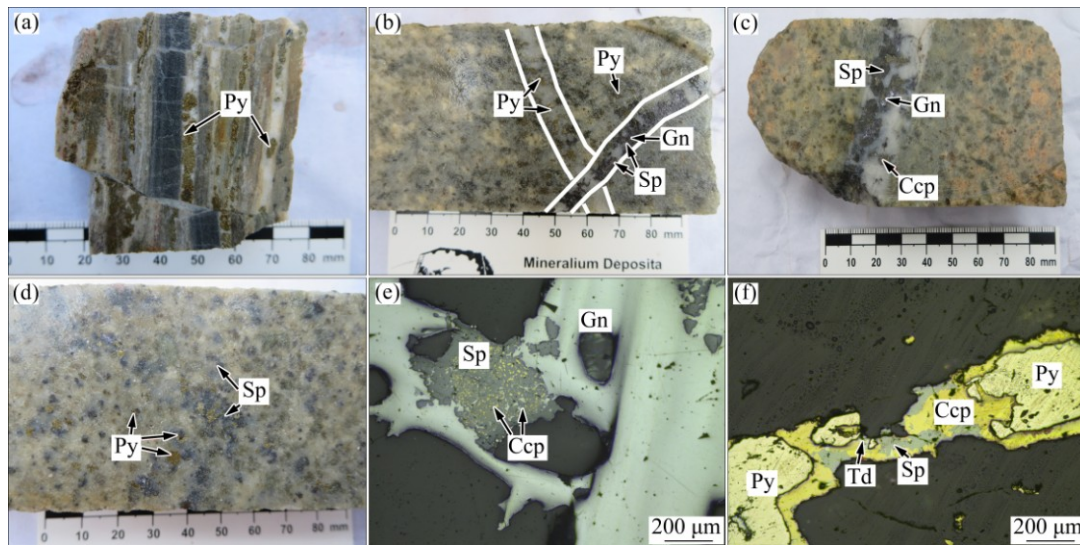


**Fig. 2** Typical ore types and microscopic images of Xiajinbao gold deposit: (a) Banded quartz–pyrite ore; (b) Quartz–galena–sphalerite vein (middle stage) intersecting cuts quartz–pyrite vein (early stage); (c) Quartz–galena–sphalerite–chalcopyrite–pyrite-bearing beresitized sericite–quartz alternated granite with quartz–galena–sphalerite–chalcopyrite–pyrite vein; (d) Disseminated-galena–pyrite-bearing sericite–quartz alternated beresitized granite with disseminated galena and pyrite; (e) Galena replacing solid solution of galena replacing chalcopyrite–sphalerite; (f) Chalcopyrite replacing pyrite, tetrahedrite and sphalerite replacing chalcopyrite

sodium feldspar, kaolinite and calcite. Based on the mineral assemblages and cross-cutting relationship of ore vein, the ore-forming process of the Xiajinbao gold deposit could be divided into three mineralization stages: the quartz–pyrite stage (early stage), quartz–galena–sphalerite stage (middle stage) and quartz–polymetallic sulfide (pyrite, chalcopyrite, galena, sphalerite, tetrahedrite) stage (late stage).

### 3 Sampling and testing methods

The isotope testing samples were collected from open pits and drilling core. The samples were selected, crushed, and processed. Pure single mineral (>95%) was selected for isotopic analysis.  $\text{Cu}_2\text{O}$  was used as the oxidizer to react with the sulfide single element to produce  $\text{SO}_2$ , which was frozen and collected for S isotopic analysis by the MAT–251 mass spectrometer. The international standard  $V_{\text{CDT}}$  was adopted. The accuracy was  $\pm 0.2\%$ , and the test was conducted by the Analytic Laboratory of BRIUG, Beijing, China.

The Pb isotope analyses were determined using an IsoProbe-T thermal ionization mass spectrometer (TIMS). Pb was separated and purified using a conventional cation-exchange technique with diluted HBr used as the eluant. The  $^{208}\text{Pb}/^{206}\text{Pb}$ ,  $^{207}\text{Pb}/^{206}\text{Pb}$ , and  $^{204}\text{Pb}/^{206}\text{Pb}$  ratios of the NBS981 Pb standard were  $2.1681 \pm 0.0008$  ( $2\sigma$ ),  $0.91464 \pm 0.00033$  ( $2\sigma$ ), and  $0.059042 \pm 0.000037$  ( $2\sigma$ ), respectively.

The H and O isotopic samples were all collected

from the drilling core. Eight pieces of single mineral samples of different stages were selected for analysis. The sizes of the granules were around  $850 \mu\text{m}$ , with purity around 99.5%. Vacuum thermal explosion method and zinc reduction method were adopted for extracting hydrogen. Under vacuum conditions, at  $500\text{--}680 \text{ }^\circ\text{C}$ ,  $\text{BrF}_5$  method was used to collect pure  $\text{O}_2$  from quartz, which was made into  $\text{CO}_2$ . The H and O isotopic analysis was conducted by the Analytic Laboratory of BRIUG using MAT–253 mass spectrometer. The error range of H isotope analysis was 0.02%, and that of O isotope analysis was 0.2%.

The samples representing different stages were selected for polishing and prepared into thermoscope-piece. Homogenization method was adopted for temperature measurement. Petrographic observation and temperature measurement of fluid inclusions were undertaken using a Linkam THMSG 600 heating–freezing stage at the Key Laboratory of Metallogenic Prediction of Nonferrous Metals and Geological Environment Monitoring, Ministry of Education, Central South University, China. Measurement has precision better than  $\pm 1 \text{ }^\circ\text{C}$  and  $\pm 0.1 \text{ }^\circ\text{C}$  in the temperature ranges of 30 to  $600 \text{ }^\circ\text{C}$  and  $-196$  to  $30 \text{ }^\circ\text{C}$ , respectively. Freezing and heating temperatures were measured using the same inclusion, where possible, and phase transitions were monitored carefully. During temperature measurement process, temperatures were changed by  $5\text{--}10 \text{ }^\circ\text{C}/\text{min}$ , and then changed slowly at steps of  $0.1\text{--}1 \text{ }^\circ\text{C}/\text{min}$  when approaching the temperature of

phase transition.

## 4 Results

### 4.1 Fluid inclusion petrography

Petrographic studies on fluid inclusions show that auriferous quartz veins are enriched in primary fluid inclusions. Based on the phase state features at room temperature, the primary fluid inclusions can be categorized into the following three types (Fig. 3).

Type I: Gas–liquid aqueous inclusions, which are composed of a little saline-water and gas bubbles under room temperature. The gas phase accounts for 10%–50% of the total volume. The size ranges from 3.9 to 10.8  $\mu\text{m}$ . The inclusions are elliptical, sub-rounded and irregular in shape, and are scattered among the quartz granules. They are well developed in all mineralization stages.

Type II:  $\text{H}_2\text{O}$ – $\text{CO}_2$  inclusions, which are made up of 3 phases at room temperature. The  $\text{CO}_2$  phase accounts for 10%–35% of the total volume. The gaseous  $\text{CO}_2$  accounts for 10%–40% of the total  $\text{CO}_2$  phase. The size ranges from 4.9 to 8.4  $\mu\text{m}$ . This type of inclusions are developed in the quartz–pyrite stage associated with type I inclusions.

Type III: Pure  $\text{CO}_2$  inclusions, which are made up of  $\text{CO}_2$  in two phases under room temperature. The gaseous  $\text{CO}_2$  accounts for 10%–40% of the total  $\text{CO}_2$ . A few inclusions are in the state of single phase at room temperature and turn into the state of two phases as the

temperature reduces. The size of the inclusions ranges from 3.6 to 6.4  $\mu\text{m}$ . The inclusions are elliptical and sub-rounded in shape, and are well developed during the quartz–pyrite stage associated with type I inclusions.

### 4.2 Fluid inclusion microthermometry

The temperature measurement results of all type fluid inclusions are illustrated in Table 1. Different histograms are drawn using the homogenization temperatures and salinity data (Fig. 4).

#### 4.2.1 Quartz–pyrite stage

The fluid inclusions in the quartz–pyrite veins include the gas–liquid aqueous inclusions (type I),  $\text{H}_2\text{O}$ – $\text{CO}_2$  inclusions (type II), and pure  $\text{CO}_2$  inclusions (type III). The ice melting temperature of the gas–liquid aqueous inclusions (type I) is from  $-7.3$  to  $-3.1$   $^{\circ}\text{C}$ . The homogenization temperature is in the range of  $216$ – $308$   $^{\circ}\text{C}$ , and concentrated in the range of  $240$ – $270$   $^{\circ}\text{C}$ . The temperature is homogenized to liquid phase. Using the Flncon software [8], the calculated salinity and density are in the ranges of  $5.2\%$ – $10.9\%$  (mass fraction,  $\text{NaCl}_{\text{eqv}}$ ) and  $0.79$ – $0.92$   $\text{g}/\text{cm}^3$ , respectively. The ice melting temperature of the aqueous– $\text{CO}_2$  inclusions is in the range of  $-7.5$  to  $-2.6$   $^{\circ}\text{C}$ . The disappearing temperature of the  $\text{CO}_2$  complex is in the range of  $7.9$ – $8$   $^{\circ}\text{C}$ . The partial homogenization temperature is  $27.6$ – $30.6$   $^{\circ}\text{C}$  and the homogenization temperature till liquid phase ranges from  $264$  to  $281$   $^{\circ}\text{C}$ . The salinity and density are in the ranges of  $3.9\%$ – $4.3\%$  (mass fraction,

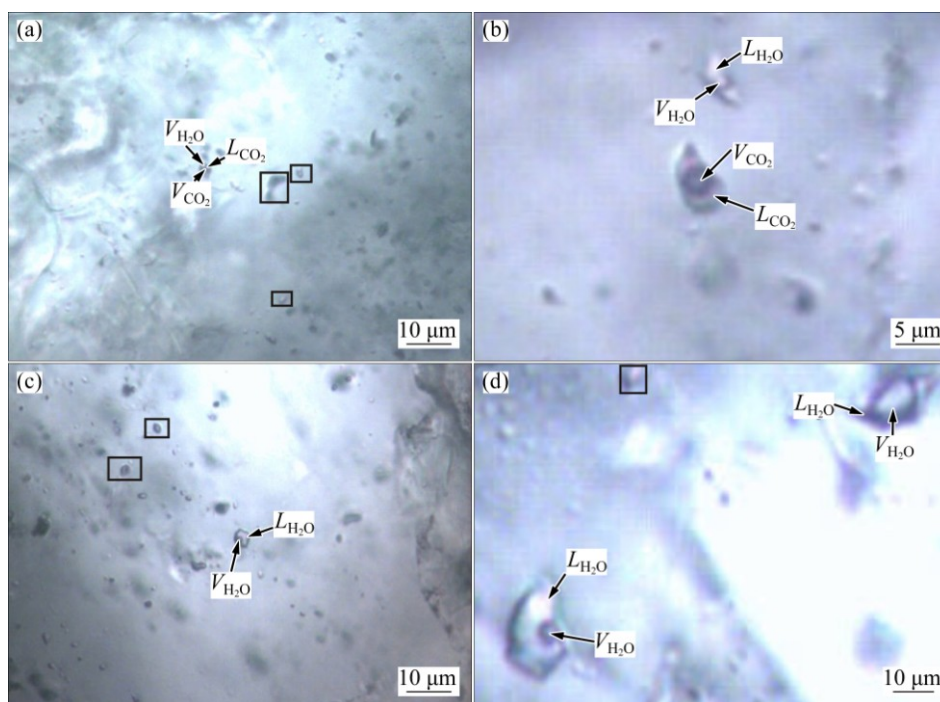


**Fig. 3** Microscopic images of all types of fluid inclusions: (a) Three-phase  $\text{CO}_2$ -rich inclusions (type II) coexisting with two-phase aqueous inclusions (type I) in early-stage veins; (b) Pure  $\text{CO}_2$  inclusions (type III) coexisting with two-phase aqueous inclusions (type I) in early-stage veins; (c) Two-phase aqueous inclusions (type I) in middle-stage veins; (d) Two-phase aqueous inclusions (type I) in late-stage veins

**Table 1** Microthermometric data of fluid inclusions in Xiajinbao gold deposit

Sample	Mineral Type	Size/ $\mu\text{m}$	$f/\%$	$t_{\text{m,CO}_2}/^\circ\text{C}$	$t_{\text{m,ice}}/^\circ\text{C}$	$t_{\text{m,Cl}}/^\circ\text{C}$	$t_{\text{h,CO}_2}/^\circ\text{C}$	$t_{\text{h}}/^\circ\text{C}$	Salinity/ $\%$	
Quartz–pyrite vein	Quartz	I	3.9–9.1	10–40				216–308	5.2–10.9	
		II	4.9–8.4	10–35	–58.5 to –55.2	–7.5 to –2.6	7.9–8.0	27.6–30.6	264–281	3.9–4.3
		III	3.6–6.4	10–40	–57.9 to –55.1			25.7–31.8		
Quartz–galena–sphalerite vein	Quartz	I	4.4–10.8	10–50				135–284	7.3–15.1	
Quartz–polymetallic sulfide vein	Quartz	I	4.6–10.0	10–50				115–194	1.0–9.6	

$f$ —Volume fraction of vapor;  $t_{\text{m,CO}_2}$ —Melting temperature of  $\text{CO}_2$ ;  $t_{\text{m,ice}}$ —Final melting temperature of ice;  $t_{\text{m,Cl}}$ —Melting temperature of  $\text{CO}_2$  clathrate;  $t_{\text{h,CO}_2}$ —Partial homogenization temperature of  $\text{CO}_2$ ;  $t_{\text{h}}$ —Homogenization temperature

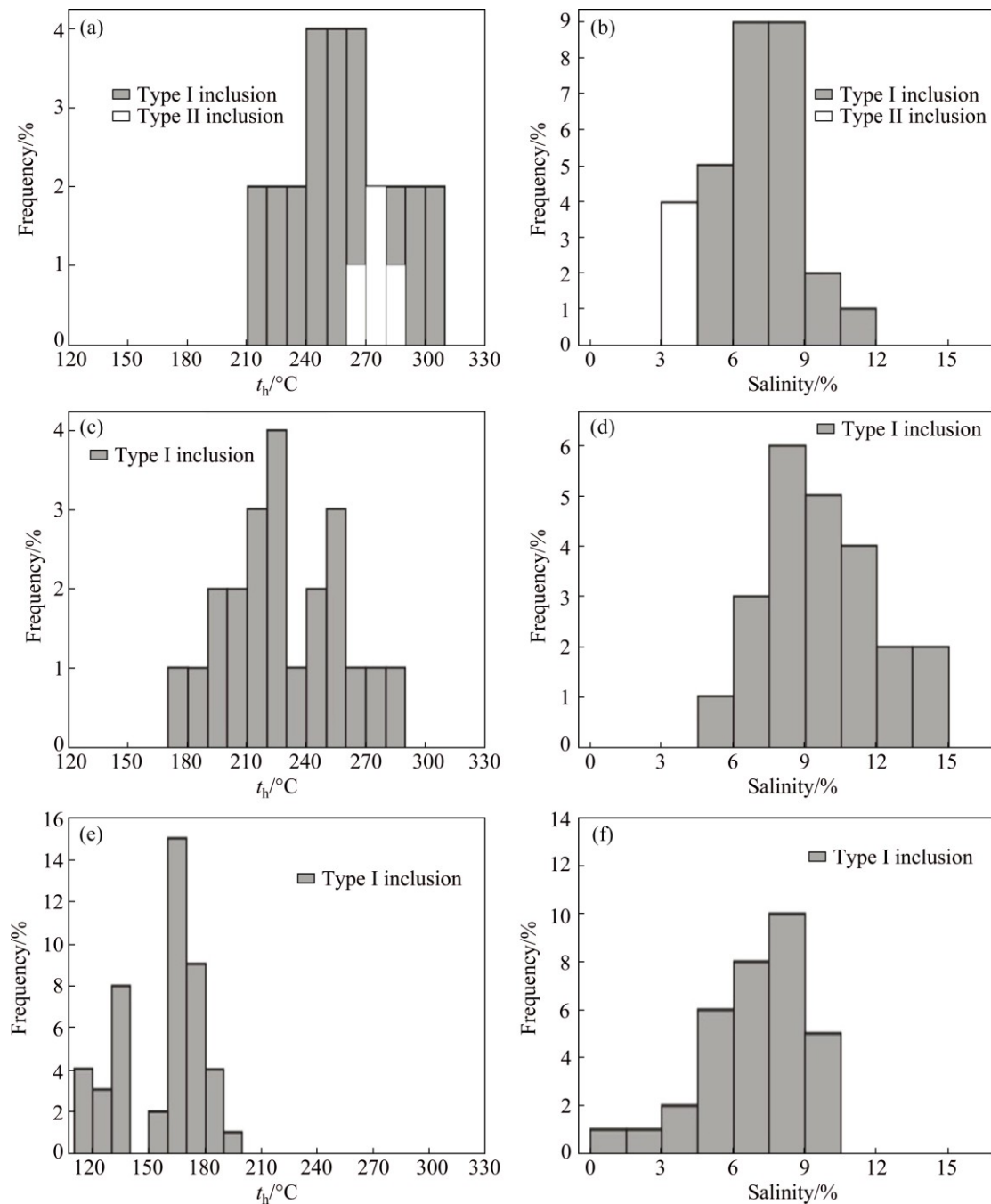


**Fig. 4** Histograms of homogenization temperature (a, c, e) and salinity (b, d, f) in fluid inclusions from Xiajinbao deposit: (a, b): Quartz–pyrite stage; (c, d): Quartz–galena–sphalerite stage; (e, f): Quartz poly-metallic sulfide stage

NaCl<sub>eqv</sub>) and 0.79–0.92 g/cm<sup>3</sup>, respectively. The three-phase point temperature of the pure inclusions is in the range of –57.9 to –55.1 °C. The temperature is homogenized to gas phase.

#### 4.2.2 Quartz–galena–sphalerite stage

Only the gas–liquid aqueous fluid inclusions (type I) are observed in the quartz–galena–sphalerite veins. The ice melting temperature of this type of inclusions is in the range of –11.1 to –6.8 °C. The homogenization temperature is in the range of 135–284 °C, and concentrated in the range of 210–240 °C. The temperature is homogenized to liquid phase. The salinity and density are in the ranges of 7.3%–15.1% (mass fraction, NaCl<sub>eqv</sub>) and 0.88–1.00 g/cm<sup>3</sup>, respectively.

#### 4.2.3 Quartz–polymetallic sulfide stage

The inclusions observed in the quartz–polymetallic sulfide stage are mainly gas–liquid aqueous inclusions (type I). The ice melting temperature is in the range of –9.8 to –6.3 °C. The homogenization temperature is in the range of 115–194 °C, and concentrated in the range of 120–180 °C. The temperature is homogenized to liquid phase, and the salinity and density are in the ranges of 1.0%–9.6% (mass fraction, NaCl<sub>eqv</sub>) and 0.94–1.00 g/cm<sup>3</sup>, respectively.

### 4.3 H and O isotopic compositions

The δ<sup>18</sup>O value for the fluid in equilibrium with the quartz could be obtained by putting the homogenization temperatures of the fluid inclusions of each mineralization stage into the equilibrium fractionation equation: δ<sup>18</sup>O<sub>Q</sub>–δ<sup>18</sup>O<sub>H<sub>2</sub>O</sub>≈3.38×10<sup>6</sup>/T<sup>2</sup>–3.40 [9]. The δD value of the fluid could be obtained by analyzing the volatile fluids entrapped in the inclusions in the veins (Table 2). The δ<sup>18</sup>O value of the fluids of the quartz–pyrite stage (early stage) is in the range of 0.726%–0.896%, and the δD value of the fluids is in the range of –9.14% to –9.10%. The δ<sup>18</sup>O value of the fluids of the quartz–galena–sphalerite stage (middle stage) is in the range of 0.234%–0.274% whereas the δD value of the fluids is in the range of –9.14% to –9.10%. The δ<sup>18</sup>O value of the fluids of the quartz–polymetallic sulfide

stage (middle stage) is in the range of –0.925% to –0.555% and the δD value of the fluids is in the range of –9.66% to –8.31%.

### 4.4 S isotopic composition features

The S isotope testing results of the Xiajinbao gold deposit are listed in Table 3. The δ<sup>34</sup>S values of the 5 pyrite samples are in the range of 0.24%–0.37%, averaging 0.326%. The δ<sup>34</sup>S values of the 5 galena samples are in the range of –0.02%–0.07%, averaging 0.022%.

### 4.5 Pb isotopic composition

The Pb isotopic composition of the Xiajinbao gold deposit is illustrated in Table 4. The <sup>208</sup>Pb/<sup>204</sup>Pb ratios of sulfides range from 35.975 to 36.204, <sup>207</sup>Pb/<sup>204</sup>Pb ranges from 15.160 to 15.231, and <sup>206</sup>Pb/<sup>204</sup>Pb ranges from 16.1 to 16.176. The related parameters of Pb isotope were calculated using the Geokit software [10], based on the measured value of <sup>208</sup>Pb/<sup>204</sup>Pb, <sup>207</sup>Pb/<sup>204</sup>Pb and <sup>206</sup>Pb/<sup>204</sup>Pb (Table 4). The Δα values range from 35.37 to 41.96, with the mean value of 39.28. The Δβ values range from –1.25 to 4.02, with the mean value of 1.78. The Δγ values range from 18.72 to 26.94, with the mean value of 23.326.

## 5 Discussion

### 5.1 Ore source

The gold ore bodies are hosted in the contact zone between the altered Xiajinbao granitic porphyry and the Archean plagioclase amphibole gneiss at the bottom of the F<sub>4</sub> fault. Gold enrichment is common in the country rock close to the granitic porphyry. The ore bodies are spatially associated with the granitic porphyry. The Au abundance of the Xiajinbao granitic porphyry is 0.018×10<sup>–6</sup>, which is 5 times higher than the Clarke value of Au, indicating that the Xiajinbao rock body has the potential to provide ore-forming materials. The Au abundance of the plagioclase amphibole porphyry is 0.029×10<sup>–6</sup>, which is 8 times higher than the Clarke

**Table 2** H and O isotope data for quartz from Xiajinbao gold deposit

Sample No.	Mineral	δD <sub>V-SMOW</sub> /‰	δ <sup>18</sup> O <sub>V-SMOW</sub> /‰	δ <sup>18</sup> O <sub>H<sub>2</sub>O-SMOW</sub> /‰	Homogenization temperature/°C
Z46-1	Quartz	–9.14	1.36	0.234	207.0
Z49	Quartz	–9.10	1.40	0.274	207.0
Z78-2	Quartz	–9.14	1.58	0.726	258.9
Z95	Quartz	–9.33	1.17	–0.595	151.5
Z124	Quartz	–9.66	1.66	0.806	258.9
Z148	Quartz	–8.31	1.21	–0.555	151.5
Z149	Quartz	–8.84	1.75	0.896	258.9
Z158	Quartz	–9.61	0.84	–0.925	151.5

**Table 3** Sulfur isotopic compositions of ore sulfides from Xiajinbao gold deposit

Sample No.	Mineral	$\delta^{34}\text{S}_{\text{V-CDT}}/\%$	Data source
K4	Pyrite	0.37	This study
K5	Pyrite	0.34	
K11	Pyrite	0.32	
K13	Pyrite	0.36	
Z33	Pyrite	0.24	
K2	Galena	0.07	
K4	Galena	0.01	
K5	Galena	-0.02	
K11	Galena	0.07	
K13	Galena	-0.02	

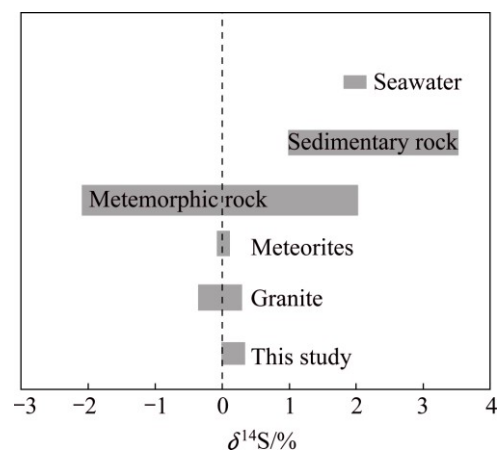
**Table 4** Lead isotopic compositions and characteristic parameters of ore sulfides from Xiajinbao gold deposit

Sample	Mineral	$^{208}\text{Pb}/^{204}\text{Pb}$	$^{207}\text{Pb}/^{204}\text{Pb}$	$^{206}\text{Pb}/^{204}\text{Pb}$	$\Delta\alpha$	$\Delta\beta$	$\Delta\gamma$
K2	Galena	36.154	15.226	16.107	41.96	4.02	26.94
K4	Galena	36.204	15.231	16.176	41.95	3.72	26.21
K5	Galena	35.975	15.160	16.106	35.37	-1.25	18.72
K11	Galena	36.099	15.197	16.157	38.70	1.20	22.25
K13	Galena	36.050	15.190	16.100	38.42	1.21	22.51

value of Au. The Au abundance of the quartz sandstone is  $0.005 \times 10^{-6}$ , which is 1.4 times higher than the Clarke value of Au. The Au abundance of the rhyolitic breccia is  $0.006 \times 10^{-6}$ , which is 1.7 times higher than the Clarke value of Au. The general gold bearing of country rock is favorable for Au mineralization.

The S isotope composition of the auriferous sulfides reveals that the  $\delta^{34}\text{S}$  values of pyrite are higher than those of the galena, suggesting that the sulfur isotopic fraction among different sulfide minerals has reached a state of equilibrium, according to the diminishing law of  $\delta^{34}\text{S}$  values of symbiotic sulfides (including sulfate) in hydrothermal system [11]. OHMOTO [12] held that the  $\delta^{34}\text{S}$  value of hydrothermal minerals is a function of the  $\delta^{34}\text{S}$  values of hydrothermal fluid, oxygen fugacity ( $f_{\text{O}_2}$ ), temperature, pH, ionic strength, i.e.,  $\delta^{34}\text{S}_{\text{mineral}} = f(\delta^{34}\text{S}_{\Sigma\text{S}}, f_{\text{O}_2}, T, \text{pH}, I)$ . The  $\delta^{34}\text{S}$  values of hydrothermal minerals depend on not only the  $\delta^{34}\text{S}$  values of the source region material but also the physical and chemical conditions during migration and precipitation of the S-bearing materials in hydrothermal fluid. OHMOTO and RYE [13] held that the  $\delta^{34}\text{S}$  values of hydrothermal fluid should be similar to those of sulfides, namely  $\delta^{34}\text{S}_{\Sigma\text{S}} \approx \delta^{34}\text{S}_{\text{sulfide}}$ , in a hydrothermal system with a relatively simple mineral assemblage in the absence of sulfates. No sulfate minerals were found in the Xiajinbao gold deposit, and the mineral composition is relatively

simple, mainly quartz, pyrite, galena, and sphalerite and chalcopyrite. Therefore, the test results of sulfide could be used to represent the total sulfur composition of hydrothermal system. The S isotopic composition of the Xiajinbao gold deposit is  $-0.02\% \sim 0.37\%$ , fluctuating around zero. The sulfur isotope is characterized by meteoritic sulfur which belongs to deep magmatic source sulfur. The difference of sulfur isotopic composition of different metallic sulfides is small, which shows that this deposit is characterized by magmatic hydrothermal deposit. Figure 5 shows that the sulfur of the Xiajinbao gold deposit mainly originated from magma, and was subordinately provided by country rock [14].

**Fig. 5** Distribution of  $\delta^{34}\text{S}$  of ore sulfides from Xiajinbao gold deposit [14]

In the  $^{207}\text{Pb}/^{204}\text{Pb}$ – $^{206}\text{Pb}/^{204}\text{Pb}$  growth line diagram (Fig. 6(a)), the Pb isotopic data are well clustered together near the lower crust line, indicating the presence of lower crust lead. In the  $\Delta\beta$ – $\Delta\gamma$  genetic classification diagram (Fig. 6(b)) of the ores [15], the data are plotted into the area between moderate–deep metamorphic lead and orogenic lead, indicating that the sources of the lead in the ore-forming materials are complicated. Both magma and strata might have been involved in the ore-forming process.

## 5.2 Source and evolution of ore-forming fluids

The  $\delta^{18}\text{O}_{\text{H}_2\text{O}}$  value of the quartz during the early mineralization period is in the range of  $0.726\% \sim 0.896\%$ , which is consistent with the O isotopic composition ( $0.55\% \sim 0.95\%$ ) of magmatic water as defined by SHEPPARD [16]. The  $\delta^{18}\text{O}_{\text{H}_2\text{O}}$  values of the quartz during the middle and late stages range from  $0.234\%$  to  $0.274\%$  and from  $0.925\%$  to  $-0.555\%$ , respectively, which are consistent with the O isotope composition of meteoric water, indicating that the meteoric water composition increases significantly along with the mineralization. In the  $\delta D$ – $\delta^{18}\text{O}_{\text{H}_2\text{O}}$  plot (Fig. 7) [17], with the evolution from early mineralization stage to late

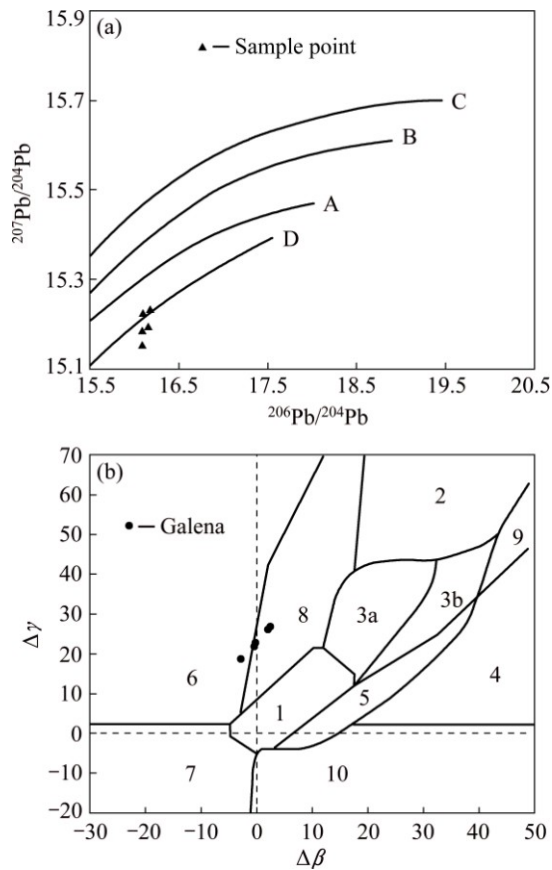


**Fig. 6**  $^{207}\text{Pb}/^{204}\text{Pb}$ – $^{206}\text{Pb}/^{204}\text{Pb}$  (a) and  $\Delta\gamma$ – $\Delta\beta$  (b) diagrams of genetic classification of ores of Xiajinbao gold deposit [15] (A—Mantle; B—Orogenic; C—Upper crust; D—Lower crust; 1—Mantle-derived; 2—Upper crust; 3—Mantle and upper crust mixed subduction zone (3a—Magmatism, 3b—Sedimentation); 4—Chemistry sediments; 5—Hydrothermal sediments on seafloor; 6—Middle to deep metamorphism; 7—Deep metamorphism lower crust; 8—Orogenic belt; 9—Upper crust of old shale; 10—Retrogressive metamorphism)

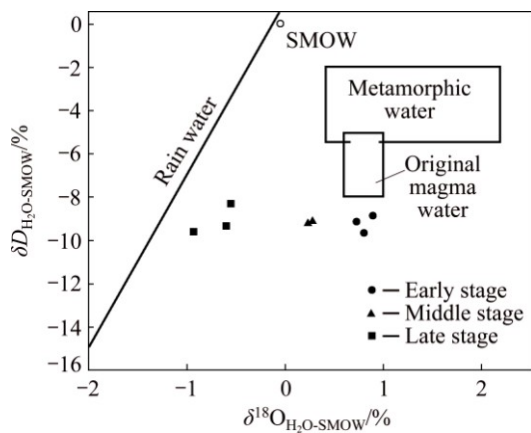


**Fig. 7**  $\delta D$ – $\delta^{18}\text{O}$  plot of Xiajinbao gold deposit [17]

mineralization stage, the  $\delta^{18}\text{O}$  values of the ore-forming fluid decrease and drift towards the meteoric water line, indicating that the ore-forming fluid was derived from magmatic water. This indicates that the meteoric water

mixed with the magmatic water gradually as the mineralization went on.

Type I inclusions are well developed during the quartz–pyrite stage. Type I inclusions co-exist with type II and type III inclusions within a very small view (Fig. 3). Type I and type II inclusions have similar homogenization temperatures, but the salinities of the two types show obvious difference (Fig. 8), indicating that the fluid inclusions were entrapped in a heterogeneous fluid system. The ore-forming fluid might have experienced boiling process during the formation of the quartz veins [18]. The salinity–enthalpy diagram plays an important role in the study of ore-forming mechanism and is effective in distinguishing the mixing from the boiling process of the ore-forming fluid [19,20]. Heat enthalpy is calculated from Harr’s equation [21] and plotted into the salinity–enthalpy diagram together with corresponding salinities (Fig. 9). The results indicate that the enthalpy is negatively correlated with the salinity values during the early stage, suggesting that the fluid has experienced a boiling process [22]. The  $\delta D$  values of all stages fall into a small range and are overall lower than the values of the granitic magmatic water

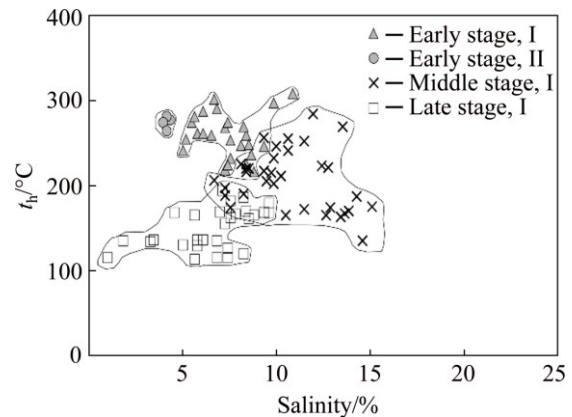


**Fig. 8** Homogeneous temperature–salinity plot of fluid inclusions of different stages

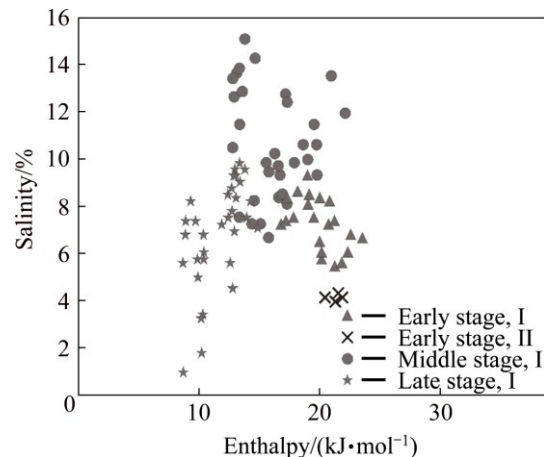


**Fig. 9** Salinity–enthalpy plot for fluid inclusions of different stages from Xiajinbao gold deposit

( $\delta^{18}D_{SMOW}$  from  $-5\%$  to  $-8\%$  [23]). The fluid moves up to the shallow altitude and the pressure declines dramatically, resulting in a boiling process during the early stage. Isotopic fractionation occurs between the vapor phase and the liquid phase and the gas escapes along the fractures, leading to relatively low  $\delta D$  values of the fluid [24,25].

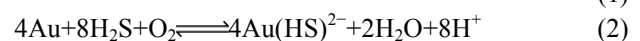
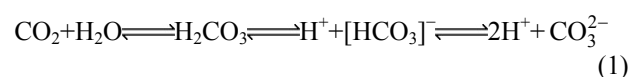
Only type I fluid inclusions are observed in the quartz–galena–sphalerite stage (middle stage). The homogenization temperature ranges from 135 to 284 °C, the salinity varies from 7.3% to 15.1% (mass fraction,  $NaCl_{eqv}$ ), and the density ranges from 0.88 to 1.00 g/cm<sup>3</sup>. The temperature of the ore-forming fluid decreases to some extent from the early stage to the middle stage, while the salinity increases, which might have resulted in CO<sub>2</sub> phase separation, caused by the boiling effect of the fluid.

Only type I fluid inclusions are found in the quartz–polymetallic sulfide stage too. The homogenization temperature ranges from 115 to 194 °C, the salinity varies from 1.0% to 9.6% (mass fraction,  $NaCl_{eqv}$ ), and the density ranges from 0.76 to 0.89 g/cm<sup>3</sup>. The temperature, salinity and density are all lower than those of the middle stage, which may result from fluid mixing with a low-temperature, low-salinity and low-density fluid. The salinities of the fluid inclusions of the middle and late stages vary in a wide range. And there is a clear linear relationship between the homogenization temperature and the salinity, and specifically, the salinity decreases as the temperature decreases (Fig. 8), which indicates that there might be a mixing process between the moderate-temperature, moderate-salinity fluid and the low-temperature, low-salinity fluid [26]. In the salinity–enthalpy diagram (Fig. 9), the enthalpy and the salinity of the middle and late stages are positively correlated, suggesting that the fluid has experienced a mixing effect [22]. The H and O isotope tracing analysis results also indicate that the ore-forming fluid might have mixed with meteoric water during the middle and late mineralization stages.

### 5.3 Ore-forming mechanism

YUAN et al [6] conducted analysis on the fission tracking age of the zircon and apatite in the ores of the Xiajinbao deposit. The metallogenic age in this area is a bit later than the age of granite porphyry ((158.0±2.5) Ma) [7], indicating that the mineralization is temporally associated with petrogenetic event. This indicates that the mineralization and the petrogenetic event are a continuum, and they are the results of the same tectonic–magmatic event under the same geodynamic setting. The rock- and ore-forming events took place during the transition period from the Paleo–Asian tectonic system to the Pacific rim tectonic

system [27,28]. The transition in geodynamic setting from compression to extension led to the underplating of basaltic magma, the partial melting of crustal materials, and the formation of granitic magma chamber. The primitive magma intruded along the intersection of the EW-trending and the NE-trending deep faults. During the late stage of the magmatic crystallization evolution, the magmatic hydrothermal fluid was derived from the magma. The hydrothermal fluid migrated along the fissures formed during the tectonic–magmatic activities, leached the ore-forming materials from the pluton and wall-rock, and evolved to form the early ore-forming fluid of the Xiajinbao deposit. In a medium–low temperature condition, gold migrates in the form of Au–S(H) complex such as  $Au(HS)_2^-$  [29,30]. The early moderate-temperature, medium–low-salinity ore-forming fluid experienced tectonic movements (especially faulting) and the temperature and pressure of the ore-forming fluid decreased dramatically, causing the boiling effect of the ore-forming fluid. The boiling effect led to the escaping of CO<sub>2</sub>, pushing the chemical equilibrium to the left. The concentration of the H<sup>+</sup> decreased and lots of S<sup>2-</sup> were formed, leading to a rise in pH. The solubility of gold complex in the hydrothermal fluid increased as a result [31]. Due to the fact that the solubility of CO<sub>2</sub> is lower than that of H<sub>2</sub>S, as the boiling effect continued, the escaping volatile shifted from CO<sub>2</sub> to H<sub>2</sub>S. The escaping of H<sub>2</sub>S impelled the chemical equilibrium to the left, and destroyed the stability of the  $Au(HS)_2^-$  complex, leading to the precipitation of gold [32,33]. Meanwhile, the S<sup>2-</sup> in the fluid combined with the Fe<sup>2+</sup> to form pyrite in the auriferous quartz–pyrite veins. During the middle and late stages, as the participation of meteoric water increased, oxidation during the mixing of fluids and escaping of H<sub>2</sub>S may account for the precipitation of Au which migrated in the form of sulfide complex [34]. Those remaining S<sup>2-</sup> in the fluid combined with the cations including Cu<sup>2+</sup>, Fe<sup>2+</sup>, Pb<sup>2+</sup> and Zn<sup>2+</sup> to form sulfides like chalcopyrite, galena and sphalerite. PHILLIPS and EVANS [35] concluded that the water/rock reaction might cause changes in the physical–chemical state of the ore-forming fluid like temperature, pressure, oxygen fugacity and pH, which could lead to the decreasing solubility of the gold complex in the ore-forming fluid and the precipitation of gold in a short time frame and a narrow space frame and the disseminated ores and the large-scale alteration formed, which is confirmed by geological facts.



As the temperature continued to decrease and the

participation of meteoric water increased, the ore-forming fluid was diluted to form barren quartz–carbonate vein, which symbolizes the end of the ore-forming process.

## 6 Conclusions

1) The macroscopic geological features of the deposit and the S, Pb isotopic tracing results indicate that the ore-forming materials of the Xiajinbao gold deposit are mainly derived from the Xiajinbao granitic magma and partly from the wall rock. The Xiajinbao granitic porphyry is the ore-forming parent rock of the Xiajinbao gold deposit.

2) The  $\delta D_{\text{H}_2\text{O-SMOW}}$  values of the ore-forming hydrothermal fluid range from  $-9.66\%$  to  $-8.31\%$ . The  $\delta^{18}\text{O}_{\text{H}_2\text{O-SMOW}}$  values range from  $-0.51\%$  to  $1.089\%$ . The H and O isotope composition features demonstrate that the ore-forming fluid is mainly derived from the magmatic hydrothermal fluid in the early stage and mixed by the meteoric water in the late stage.

3) The ore-forming fluid experienced boiling effect during the quartz–pyrite stage, causing the salinity of the fluid to tend to increase. The escaping of volatiles like  $\text{CO}_2$  and  $\text{H}_2\text{S}$  leads to the decreasing stability of the  $\text{Au}(\text{HS})^{2-}$  complex in the fluid and the precipitation of gold. The ore-forming fluid mixed with the meteoric water during the middle and late stages, which resulted in decreasing salinity and density of the fluid. The oxidation during the mixing process and the loss of  $\text{H}_2\text{S}$  become the major cause for the precipitation of gold. The water/rock reaction caused the changes in the physical–chemical conditions of the ore-forming fluid and the precipitation of gold throughout the whole ore-forming process.

## References

- [1] LUAN Wen-lou, YU Yao-xian. Geochemistry of fluid inclusion of Xiayingfang gold deposit in Pingquan of Hebei province and ore-searching significance [J]. *Journal of Precious Metallic Geology*, 1995, 4(3): 161–167. (in Chinese)
- [2] HUANG Dian-hao, WU Cheng-yu, DU An-dao, HE Hong-liao. Re–Os ages molybdenum deposits in east Qinling and their significance [J]. *Mineral Deposits*, 1996, 13(3): 221–230. (in Chinese)
- [3] HUANG Dian-hao, DONG Qun-ying, GAN Zhi-xian. China molybdenum deposits [M]. Beijing: Geological Publishing House, 1989: 493–536. (in Chinese)
- [4] RUI Zong-yao, HUANG Chong-ke, QI Guo-ming, XU Jue, ZHANG Hong-tao. Porphyry copper (molybdenum) deposits of China [M]. Beijing: Geological Publishing House, 1984: 1–350. (in Chinese)
- [5] PEI Rong-fu, LÜ Feng-xiang, FAN Ji-zhang, FANG Rui-heng, QI Chao-shun. Metal deposits metallogenetic series and prospecting of north margin of the North China massif and its north side [M]. Beijing: Geological Publishing House, 1998: 1–237. (in Chinese)
- [6] YUAN Wan-ming, WANG Shi-cheng, WANG Lan-fen. Fission track study on the metallogenetic age of Xiayingfang gold deposit in eastern, Hebei [J]. *Nuclear Techniques*, 1999, 22(7): 411–413. (in Chinese)
- [7] ZHANG Jian-guo, SHAO Yong-jun, LIU Zhong-fa, WANG Cheng, ZOU Yan-hong, LI Hong-bin. Zircon U–Pb geochronology and Hf isotope characteristics of Xiajinbao granite–porphyry body, Hebei Province, and its geological significance [J]. *Transactions of Nonferrous Metals Society of China*, 2016, 26(1): 137–148.
- [8] BROWN P E. FLINCOR: A microcomputer program for the reduction and investigation of fluid-inclusion data [J]. *American Mineralogist*, 1989, 74: 1390–1393.
- [9] CLAYTON R N, O'NEIL J R, MAYEDA T K. Oxygen isotope exchange between quartz and water [J]. *Journal of Geophysical Research*, 1972, 77(17): 3057–3067.
- [10] LU Yuan-fa. Geokit—A geochemical toolkit for Microsoft Excel [J]. *Geochimica*, 2004, 33(5): 459–464. (in Chinese)
- [11] ZHANG Li-gang. The application of the stable isotope to geology [M]. Xi'an: Xi'an Science and Technology Press: 1985: 1–267. (in Chinese)
- [12] OHMOTO H. Systematics of sulfur and carbon isotopes in hydrothermal ore deposits [J]. *Economic Geology*, 1972, 67(5): 551–578.
- [13] OHMOTO H, RYE R O. Isotope of sulfur and carbon — Geochemistry of hydrothermal ore deposits [M]. 2nd ed. New York: John Wiley and Sons, 1979: 509–561.
- [14] HOU Dong-zhuang, WU Xiang-bin, LI Zhen, LIU Yu-hong. Ore-forming material sources of Dahebian barite deposit in Tianzhu county, Guizhou Province, China [J]. *The Chinese Journal of Nonferrous Metals*, 2015, 25(4): 1039–1048. (in Chinese)
- [15] ZHU Bing-quan, LI Xian-hua, DAI Tong-mo. System theory application of isotopes in the earth sciences: On the Chinese mainland crust–mantle evolution [M]. Beijing: Science Press, 1998: 224–226. (in Chinese)
- [16] SHEPPARD S M F. Characterization and isotopic variations in natural waters [J]. *Review in Mineralogy and Geochemistry*, 1986, 16(3): 165–183.
- [17] PENG Nan-hai, SHAO Yong-jun, LIU Zhong-fa, WANG Cheng. Metallogenic mechanism of Yixingzhai gold ore field in Fanshi county, Shanxi province: Evidences from isotopes and fluid inclusion [J]. *The Chinese Journal of Nonferrous Metals*, 2017, 27(2): 305–317. (in Chinese)
- [18] LU Huan-zhang, FAN Hong-rui, NI Pei, OU Guang-xi, SHEN Kun, ZHANG Wen-huai. Fluid inclusions [M]. Beijing: Science Press, 2004: 400–419. (in Chinese)
- [19] HEDENQUIS J W. The thermal and geochemical structure of the Broadlands-Ohaaki geothermal system, New Zealand [J]. *Geothermics*, 1990, 19(2): 151–185.
- [20] ZHANG Wen-huai, ZHANG De-hui, LIU Min. Study on ore-forming fluids and the ore-forming mechanisms of the Yinshan Cu–Pb–Zn–Au–Ag deposits, Jiangxi province [J]. *Acta Petrologica Sinica*, 2003, 19(2): 242–250. (in Chinese)
- [21] HAAR L, GALLAGHER J S, KELL G S. NBS/NRC steam tables: Thermal dynamic and transport properties and computer program for vapor and liquid states of water in SI units [M]. Washington D C: Hemisphere Publishing Corp, 1984: 1–136.
- [22] WILKINSIN J J. Fluid inclusions in hydrothermal ore deposits [J]. *Lithos*, 2001, 55(1–4): 229–272.
- [23] TAYLOR H P. Oxygen and hydrogen isotope studies of plutonic granitic rocks [J]. *Earth and Planetary Science Letters*, 1978, 38(1): 177–210.
- [24] NABLEK P I, O'NEIL J R, PAPIKEOR J J. Vapor phase exsolution as a controlling factor in hydrogen isotope variation in granitic rocks: The Notch Peak granitic stock, Utah [J]. *Earth Planet*, 1983, 66: 137–150.

- [25] SHMULOVIC A L, LADWEHR D, SIMON K, HEINRICH W. Stable isotope fraction between liquid and vapor in water-salt system up to 600 °C [J]. *Chemical Geology*, 1999, 157: 343–354.
- [26] XIONG Yi-qu, SHAO Yong-jun, LIU Jian-ping, WEI Han-tao, ZHAO Rui-cheng. Ore-forming fluid of quartz-vein type tungsten deposits, Xitian ore field, eastern Hunan, China [J]. *The Chinese Journal of Nonferrous Metals*, 2016, 26(5): 1107–1119. (in Chinese)
- [27] MAO Jing-wen, ZHANG Zuo-heng, YU Jin-jie, NIU Bao-gui. The geodynamic setting of Mesozoic large scale mineralization in North China: The revelation from accurate timing of metal deposits [J]. *Science in China (Series D)*, 2003, 33(4): 289–300. (in Chinese)
- [28] MAO Jing-wen, XIE Gui-qing, ZHANG Zuo-heng, WANG Yi-tian, ZHANG Chang-qing, LI Yong-feng. Mesozoic large-scale metallogenic pulses in North China and corresponding geodynamic settings [J]. *Acta Petrologica Sinica*, 2005, 21(1): 169–188. (in Chinese)
- [29] HAYASHI K, OHMOTO H. Solubility of gold in NaCl and H<sub>2</sub>S-bearing aqueous solutions at 250 °C–350 °C [J]. *Geochimica Cosmochimica Acta*, 1991, 55: 2111–2126.
- [30] COLE D R, DRUMMOND S E. The effect of transport and boiling on Ag/Au ratios in hydrothermal solutions: A preliminary in ray assessment and possible implications for the formation of epithermal precious metal ore deposits [J]. *Journal of Geochemical Exploration*, 1986, 25: 45–79.
- [31] DRUMMOND S E, OHMOTO H. Chemical evolution and mineral deposition in boiling hydrothermal systems [J]. *Economic Geology*, 1985, 80: 126–147.
- [32] REED M H, SPYCHER N F. Boiling, cooling and oxidation in epithermal systems: A numerical modeling approach [J]. *Reviews in Economic Geology*, 1985, 2: 249–272.
- [33] SPYCHER N F, REED M H. Evolution of a broad lands-type epithermal ore fluid along alternative P-T paths: Implication for the transport and deposition of base, precious and volatile metals [J]. *Economic Geology*, 1989, 84: 328–359.
- [34] ZHANG De-hui. Some new advances in ore-forming fluid geochemistry on boiling and mixing of fluid during the processes of hydrothermal deposits [J]. *Advance in Earth Sciences*, 1997, 12(6): 546–552. (in Chinese)
- [35] PHILLIPS G N, EVANS K. A Role of CO<sub>2</sub> in the formation of gold deposits [J]. *Nature*, 2004, 429: 860–863.

## 基于流体包裹体及稳定同位素的 河北平泉下金宝金矿床成矿机理

张建国<sup>1,2,3</sup>, 邵拥军<sup>1,2</sup>, 汪程<sup>1,2</sup>, 刘忠法<sup>1,2</sup>, 熊伊曲<sup>1,2</sup>

1. 中南大学 有色金属成矿预测与地质环境监测教育部重点实验室, 长沙 410083;
2. 中南大学 地球科学与信息物理学院, 长沙 410083;
3. 中国有色金属矿产地质调查中心, 北京 100012

**摘要:** 下金宝金矿床位于永安—下营房—毛家沟金多金属成矿带。本文作者以河北下金宝金矿床流体包裹体和稳定同位素为研究对象, 分析了本区成矿物质来源、成矿流体来源及其演化, 进而探讨本矿床的成矿机理。宏观地质特征和 S、Pb 同位素示踪结果表明, 本区成矿物质主要由下金宝花岗质岩浆提供, 部分来源于围岩。H、O 同位素组成特征显示, 本区成矿流体来源于岩浆水。流体包裹体特征表明, 本区早阶段的成矿流体在演化过程中发生了沸腾作用, 导致金的沉淀, 中、晚阶段成矿物质沉淀的主导因素为流体的混合作用, 而水/岩反应促使金沉淀的现象贯穿成矿的始终。

**关键词:** 流体包裹体; 稳定同位素; 成矿物质来源; 成矿机理; 下金宝金矿床

(Edited by Wei-ping CHEN)